Is axial dispersion within rotating cylinders governed by the Froude number?

J. R. Third* and C. R. Müller
Institute of Energy Technology, Department of Mechanical and Process Engineering, ETH Zürich, Leonhardstrasse 27, 8092 Zürich, Switzerland
(Received 24 July 2012; published 21 December 2012)

Axial dispersion rates of particles within horizontal rotating cylinders have been calculated for a decade of cylinder diameters. Throughout the range studied the rate of axial dispersion was found to be independent of the cylinder diameter. This phenomenon has been investigated further by spatially resolving the local contribution to the axial dispersion coefficient. This analysis demonstrates that, although the highest rates of axial dispersion occur at the free surface of the bed, there is a significant contribution to axial dispersion throughout the flowing region of the bed. Finally, based on an analogy with a Galton board, a linear relationship is proposed between the local rate of axial dispersion within a horizontal rotating cylinder and the product of the local particle concentration and the local shear rate in a plane perpendicular to the cylinder axis.

DOI: 10.1103/PhysRevE.86.061314 PACS number(s): 45.70.Mg, 83.10.Rs, 83.80.Fg

I. INTRODUCTION

The motion of particles within partially filled, horizontal, rotating cylinders has attracted significant academic interest in recent years [1–6]. These systems are also of significant importance in industry, where they find application in processes such as waste incineration, cement manufacture, and the production of titanium dioxide. One area that is of both academic and industrial interest is axial dispersion within rotating cylinders [7,8].

Axial dispersion within horizontal rotating cylinders containing glass ballotini was studied by Parker *et al.* [9] using positron emission particle tracking. Using 1.5 and 3 mm ballotini and cylinder diameters of 100, 136, and 144 mm, Parker *et al.* [9] found that the rate of axial dispersion was strongly influenced by the particle diameter but did not appear to depend on the drum diameter.

Third *et al.* [10] used the discrete element method (DEM) to calculate axial dispersion coefficients (D_{ax}) for beds composed of approximately monosized spheres. For a range of particle diameters, rotation speeds, drum diameters, and gravitational strengths, they found that their results could be described by the correlation

$$\frac{D_{\mathrm{ax}}}{d_p^{2-\lambda} g^{\lambda} \Omega^{1-2\lambda}} = K. \tag{1}$$

Here d_p is the particle diameter, g is the acceleration due to gravity, Ω is the rotation speed of the cylinder, K is a dimensionless constant, and λ is a parameter in the range 0.1–0.15. For cylinder diameters (D) between 75 and 200 mm, Third *et al.* found that D_{ax} was independent of D, whereas a smaller value of D_{ax} was obtained for a cylinder diameter of 50 mm.

Both Parker *et al.* [9] and Third *et al.* [10] found the rate of axial dispersion to be independent of the drum diameter (D) for sufficiently large values of D. This result is particularly intriguing since it implies that the rotational Froude number ($\mathrm{Fr} = \Omega^2 D/2g$), which is often used to characterize particle motion within rotating cylinders [11,12], does not govern axial dispersion within these systems. However, neither Parker *et al.* [9] nor Third *et al.* [10] were able to provide an explanation of why D_{ax} is independent of D. Furthermore, for large values of D the particle motion within the bed will move from the rolling regime observed at low Fr to the cataracting or centrifuging regimes. Therefore, although it has never been reported, it is expected that there is an upper limit for D above which the observation that D_{ax} is independent of D will fail.

In this work the DEM is used to examine the influence of cylinder diameter on axial dispersion over a decade of drum diameters. In addition, the axial displacement of particles is spatially resolved, which provides insight into how and where axial dispersion occurs within rotating cylinders. Finally, a model is proposed which links the local rate of axial dispersion in a rotating cylinder to the local shear rate.

II. SIMULATION METHOD

The soft-sphere DEM is well documented in the literature [13–16] and will not be described here except to detail the particular force laws used in this work.

The force in the normal direction F_n is modeled using a damped linear spring and attractive forces between particles are prevented. Therefore, for a collision between particles i and j, F_n is given by

$$F_n = \max\left(0, k_{n_{ij}}\delta_n - 2\eta_n\sqrt{m_{ij}k_n}v_n\right). \tag{2}$$

Here η_n is the damping factor in the normal direction, δ_n is the particle overlap, k_n is the normal stiffness, v_n is the relative velocity in the normal direction, and m_{ij} is the effective mass defined as $1/m_{ij} = 1/m_i + 1/m_j$. In the tangential direction static friction is modeled as a damped linear spring and the magnitude of the tangential force is limited by Coulomb's law such that

$$F_t = \min\left(\mu k_{n_{ij}}\delta_n, k_{t_{ij}}\delta_t - 2\eta_t\sqrt{m_{ij}k_t}v_t\right). \tag{3}$$

Here μ is the coefficient of friction, η_t is the damping factor in the tangential direction, k_t is the tangential stiffness, and v_t is the relative velocity of the two surfaces in contact. The tangential displacement δ_t is defined as $\int v_t\, dt$. Table I shows the parameter values used in this work. The fill level is defined

*jthird@ethz.ch

TABLE I. Simulation parameter values.

Parameter	Symbol	Value
Nominal particle diameter	d_p	3 mm
Particle size distribution		±5%
Particle density	ρ	2500 kg/m^3
Normal spring stiffness	k_n	1000 N/m
Tangential spring stiffness	k_t	500 N/m
Normal damping factor	η_n	0.2
Tangential damping factor	η_t	0.2
Particle coefficient of friction	μ_p	0.7
Acceleration due to gravity	g	9.81 m/s^2
Length of cylinder	L	152 mm
Cylinder rotation speed	Ω	5.8, 10, 17.3 rpm
Fill level	f	26%
Time step for numerical scheme	dt	1×10^{-5} s

as the fraction of the cylinder taken up by particles and voids between particles when the cylinder is rotating.

The cylinder in which the particles are rotated is modeled as a smooth, but frictional, cylinder onto which "wall rougheners" have been attached to prevent slip between the cylinder wall and the bed [17]. The wall rougheners consist of lines of 3 mm particles running along the length of the cylinder and they are equally spaced around the cylinder circumference with a center-to-center spacing of approximately five particle diameters. The centers of the particles making up the wall rougheners are located on the cylinder circumference. The ends of the cylinder are modeled as frictionless plane walls. With the exception of the friction coefficient of the end plates, the physical properties of the cylinder, the wall rougheners, and the end plates are identical to those of the particles. Gravity acts in a direction perpendicular to the cylinder axis for all simulations. The equations of motion are integrated using a third-order Adams-Bashforth scheme with a time step dt, which satisfies $dt \leqslant t_{\mathrm{col}}/30$, where t_{col} is the duration of a binary collision.

III. AXIAL DISPERSION

In this work axial dispersion is quantified by calculating the mean-square deviation in the axial position of a group of particles as a function of observation time, Δt. It has previously been shown that axial dispersion within horizontal rotating cylinders obeys Fick's second law [8,10], allowing the axial dispersion coefficient D_{ax} to be related to the mean-square deviation in particle position as shown by Eq. (4).

$$\frac{1}{N'}\sum_{k=1}^{N'}[z_k(t+\Delta t)-z_k(t)]^2 = 2D_{\mathrm{ax}}\Delta t. \qquad (4)$$

Here z_k is the axial position of particle k and N' is the number of particles contributing to the mean-square deviation. The dispersion coefficients presented here are calculated by computing the mean-square deviation of a 50 mm axial pulse of particles that is initially located axially in the center of the cylinder. The motion of the particles in this pulse is tracked for a 20 s time interval before a new pulse of particles is selected and the process is repeated. The results presented here are based on averaging nine such time segments, i.e., 180 s of simulated time.

TABLE II. Axial dispersion coefficients for the systems studied here. The mean of the product of the local shear rate and the local particle concentration is also shown.

Drum diameter (mm)	Ω (rpm)	Fr	D_{ax} (m^2/s)	$\overline{C\lvert\epsilon_{xy}\rvert}$ (s^{-1})
100	10.0	0.0056	3.0×10^{-6}	22.4
200	10.0	0.0112	3.0×10^{-6}	24.2
300	5.8	0.0056	1.9×10^{-6}	17.0
300	10.0	0.0168	2.9×10^{-6}	24.4
300	17.3	0.0503	4.5×10^{-6}	34.6
400	10.0	0.0224	2.9×10^{-6}	24.4
500	10.0	0.0279	3.0×10^{-6}	24.2
1000	10.0	0.0558	3.0×10^{-6}	23.1

IV. RESULTS

Table II summarizes the axial dispersion coefficients obtained for drum diameters ranging from 100 to 1000 mm. These data indicate that, for the system studied here, the drum diameter does not influence the rate of axial dispersion. For $D = 300$ mm simulations were performed at rotation speeds of 5.8, 10, and 17.3 rpm. The (dimensionless) Froude number of the 300 mm drum with a rotation speed of 5.8 rpm is the same as that of the 100 mm drum rotating at 10 rpm. Table II indicates that D_{ax} is very different for these two systems, highlighting that axial dispersion cannot be characterized by the Froude number. To understand better how and where axial dispersion occurs, the spatially resolved contribution to the axial dispersion coefficient is shown in Fig. 1 for an observation time $\Delta t = 0.2$ s. Plots are shown for the $D = 200$ and $D = 500$ mm cases. These data indicate that axial dispersion occurs predominantly in the flowing or active region of the bed and that very little dispersion occurs in the passive region close to the cylinder wall. For both bed diameters the highest rates of axial dispersion occur in a narrow band at the free surface of the bed and at the shoulder and toe of the bed. However, since these regions are relatively small compared to the total area of the flowing region, they do not dominate the total axial dispersion.

V. DISCUSSION

A Galton board consists of rows of pegs arranged on a triangular pitch through which spherical beads are dropped. When a bead collides with a peg it has an equal probability of being diverted to either the left or the right of the peg with the result that the variance in the horizontal positions of a group of beads that have passed through the board increases linearly with the number of rows of pegs in the board. Here we propose an analogy between the Galton board and the motion of particles within a horizontal cylinder by considering the bed within a horizontal cylinder to be comprised of layers of beads moving over one another with a relative velocity, v_{rel}. A sheet of spherical particles has a rough surface with peaks corresponding to the tops of spheres and troughs corresponding

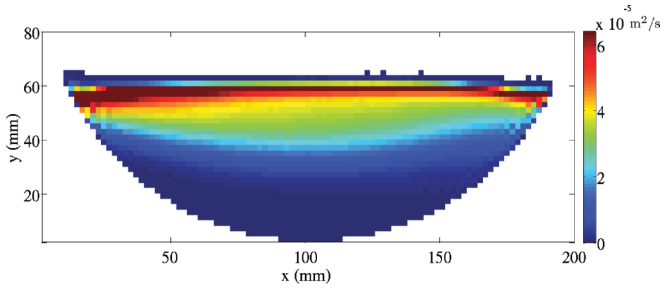

(a) D = 200 mm

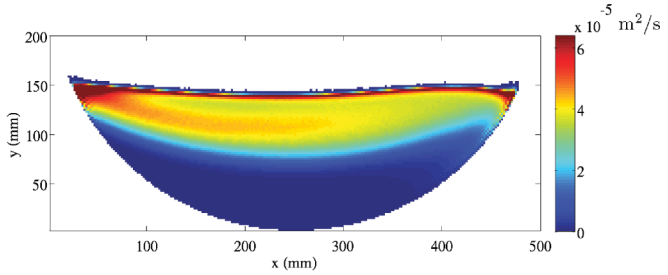

(b) D = 500 mm

FIG. 1. (Color online) Spatially resolved contribution to the axial dispersion for a voxel size of 2 mm × 2 mm × 50 mm using observation time $\Delta t = 0.2$ s. The calculation is restricted to particles initially located in a 50-mm-long axial pulse at the center of the cylinder and the data have been averaged over 180 s of simulated time. The beds have been rotated by the dynamic angle of repose of the bed such that the upper surface of the bed is horizontal. The shoulder of the bed (highest point on the free surface) is on the right of the figures.

to the gaps between spheres. The peaks on this surface can be thought of as acting in a similar manner to the pegs on a Galton board since a particle approaching a peak will tend to be diverted to the left or right in order to minimize the dilation caused by its movement across the surface. Therefore, the relative velocity between adjacent sheets of spheres will lead to particles being displaced perpendicular to v_{rel}, just as particles undergo a horizontal displacement as they descend a Galton board.

This analogy suggests that the local contribution to the axial dispersion coefficient should be proportional to v_{rel} since this will govern how many "pegs" the particles will collide with per second. Therefore, it is proposed here that the local contribution to the axial dispersion coefficient is proportional to the product of the local particle concentration and the local shear rate in the x-y plane, Eq. (5).

$$\frac{1}{2V_{\text{vox}}\Delta t}\sum[z_k(t+\Delta t)-z_k(t)]^2 = kC|\epsilon_{xy}|. \qquad (5)$$

Here V_{vox} is the volume of the voxels used to resolve the axial dispersion, C is the local particle concentration, ϵ_{xy} is the local shear rate, and k is a proportionality constant.

Figure 2 plots the local contribution to the axial dispersion coefficient as a function of the product of the local particle concentration and the local shear rate for drum diameters of 200 and 500 mm. The local shear rates were calculated from time-averaged velocity profiles as $\frac{1}{2}|\frac{\partial u}{\partial y}+\frac{\partial v}{\partial x}|$ and finite

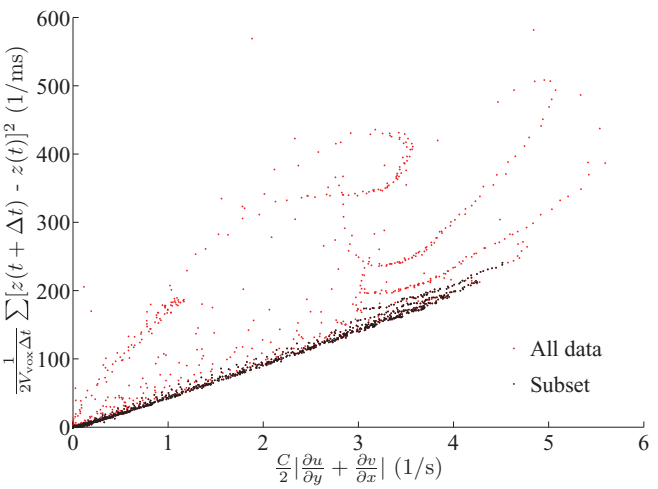

(a) D = 200 mm

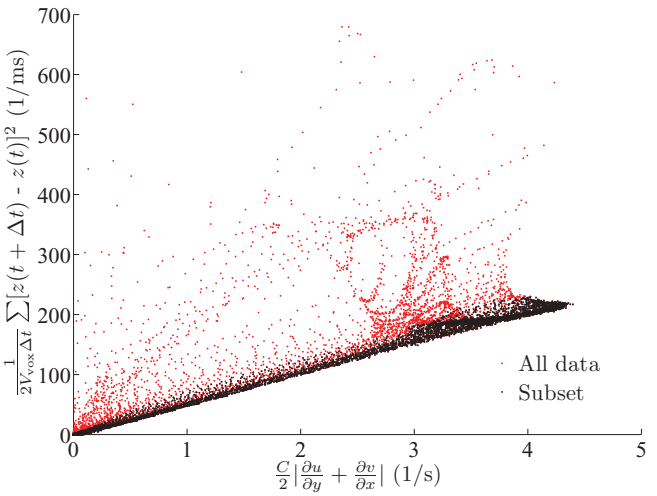

(b) D = 500 mm

FIG. 2. (Color online) Scatter plots showing the local contribution to D_{ax} against $C|\epsilon_{xy}|$. Data are shown for drum diameters of 200 and 500 mm.

differences were applied to approximate the derivatives. From Fig. 2 it can be seen that many of the data for both drum diameters shown lie on a straight line that passes through the origin and has a slope of $k = 48$ m^{-1}, which demonstrates the functional form proposed in Eq. (5). Furthermore, no data lie below this line, indicating that Eq. (5) provides a lower bound for the local contribution to the dispersion coefficient. A similar trend is observed for the other drum diameters. Table II shows the mean of the product of the local particle concentration and the local shear rate for all the simulations reported here.

To identify the regions of the bed where Eq. (5) underestimates the dispersion rate, the local contribution to D_{ax} predicted by Eq. (5) is plotted in Fig. 3 for $k = 48$ m^{-1} and a voxel size of 2 mm × 2 mm × 50 mm. Data are shown for drum diameters of 200 and 500 mm. These data indicate good agreement between the calculated local dispersion rates and those predicted by Eq. (5) for large portions of both beds. The largest discrepancies between the model and the calculated values are coincident with the regions of highest

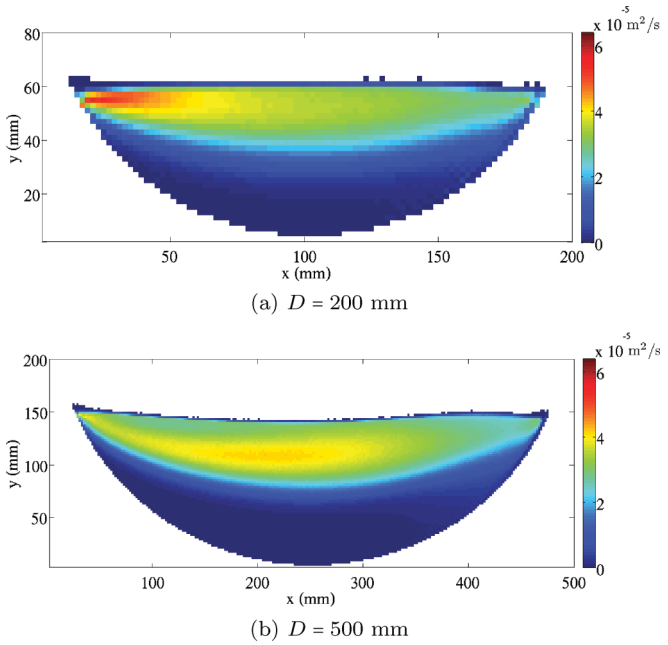

FIG. 3. (Color online) Local contribution to D_{ax} predicted by Eq. (5) with $k = 48\ \mathrm{m}^{-1}$ and a voxel size of 2 mm × 2 mm × 50 mm.

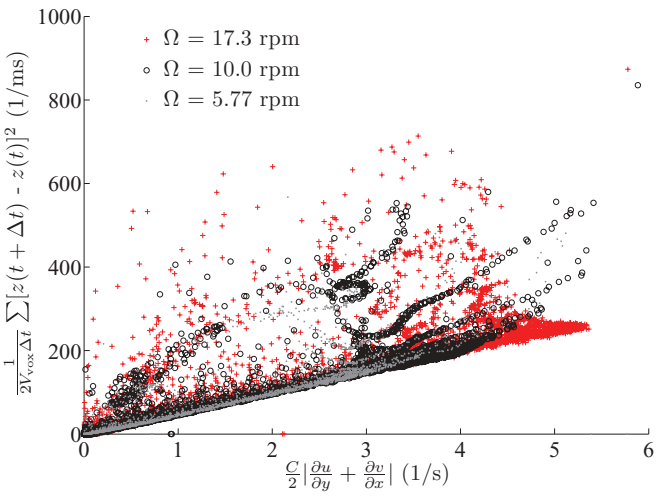

FIG. 4. (Color online) Scatter plot showing the local contribution to D_{ax} against $C|\epsilon_{xy}|$. The drum diameter is 300 mm and data are shown for rotation speeds of 5.8, 10, and 17.3 rpm.

axial dispersion, i.e., on the free surface and the shoulder and toe of the bed. To confirm that deviations from Eq. (5) are predominantly located in these regions, the local contribution to the axial dispersion coefficient was plotted against the product of the local particle concentration and the local shear rate for areas excluding the free surface and the shoulder and toe of the bed. These data, termed the "subset," are shown in Fig. 2 for drum diameters of 200 and 500 mm. For $D = 200$ mm the subset was defined as 40 mm $< x <$ 160 mm, $y < 52$ mm and for $D = 500$ mm the subset was defined as 100 mm $< x < 400$ mm, $y < 130$ mm. Figure 2 shows good agreement between the subset and Eq. (5) for both drum diameters, confirming that deviations from this linear behavior are largely located at the free surface and at the shoulder and toe of the bed. A possible explanation for this deviation may be as follows: Particles located on the free surface of the bed are less constrained than particles within the bulk since they have no particles above them. This difference may result in a different relationship between shear rate and axial dispersion for these particles. At the toe of the bed the particles undergo a deceleration approximately parallel to the free surface of the bed and there is a similar acceleration at the shoulder of the bed. These accelerations will produce additional strain rates (predominantly ϵ_{xx}), which may result in additional axial dispersion. However, a quantitative analysis of the influence of ϵ_{xx} is beyond the scope of this paper.

Equation (5) was proposed without a detailed consideration of the particle motion within the cylinder. Therefore, this relation should be expected to hold for a range of operating conditions. Above we have demonstrated that, away from the free surface and from the shoulder and toe of the bed, Eq. (5) appears to hold for a large range of D and that the proportionality constant k is independent of D. To demonstrate further the robustness of this relation, the effect of rotation speed has been considered for $D = 300$ mm. Figure 4 shows the local contribution to the axial dispersion coefficient plotted against the product of the local particle concentration and the local shear rate for rotation speeds of 5.8, 10, and 17.3 rpm. All three rotation speeds demonstrate the same behavior observed in Fig. 2: a large number of the data are located on a straight line with a proportionality constant of $k = 48\ \mathrm{m}^{-1}$ and no data is located below this line.

The data presented in Figs. 2 and 4 indicate that there is a strong relationship between the local axial dispersion and the product of the local shear rate and the local concentration. For rotating cylinders operating in the rolling regime, particle velocities are expected to scale approximately linearly with the drum diameter [18]. Therefore, the shear rate within the cylinder, which is $O(\frac{u}{D})$, is approximately independent of the drum diameter. Thus, the data presented here suggest that the rate of axial dispersion within rotating cylinders is independent of D because the shear rate within these systems does not depend on D.

VI. CONCLUSIONS

Axial transport within horizontal rotating cylinders has been studied using the DEM for drum diameters ranging from 100 to 1000 mm. Throughout this range of D the rate of axial dispersion was found to be independent of the drum diameter. By spatially resolving the local contribution to D_{ax}, it was shown that the highest local contribution occurs on the free surface of the bed but that there is a significant contribution to D_{ax} throughout the flowing region of the bed. A model for axial dispersion within rotating cylinders operating in the rolling regime has been proposed based on an analogy with a Galton board. This model has been shown to give good agreement with calculated values for the local contribution to D_{ax} for a large portion of the bed for all drum diameters and rotation speeds studied here.

[1] I. S. Aranson, L. S. Tsimring, and V. M. Vinokur, Phys. Rev. E **60**, 1975 (1999).
[2] K. M. Hill and J. Kakalios, Phys. Rev. E **52**, 4393 (1995).
[3] D. Fischer, T. Finger, F. Angenstein, and R. Stannarius, Phys. Rev. E **80**, 061302 (2009).
[4] J. R. Third, D. M. Scott, and C. R. Müller, Phys. Rev. E **84**, 041301 (2011).
[5] D. C. Rapaport, Phys. Rev. E **65**, 061306 (2002).
[6] I. Zurriguel, J. F. Boudet, Y. Amarouchene, and H. Kellay, Phys. Rev. Lett. **95**, 258002 (2005).
[7] Z. S. Khan and S. W. Morris, Phys. Rev. Lett. **94**, 048002 (2005).
[8] N. Taberlet and P. Richard, Phys. Rev. E **73**, 041301 (2006).
[9] D. J. Parker, A. E. Djkstra, T. W. Martin, and J. P. K. Seville, Chem. Eng. Sci. **52**, 2011 (1997).
[10] J. R. Third, D. M. Scott, and S. A. Scott, Powder Technol. **203**, 510 (2010).
[11] J. F. Davidson, D. M. Scott, P. A. Bird, O. Herbert, A. A. Powell, and H. V. M. Ramsay, Kona **18**, 149 (2000).
[12] J. Mellmann, Powder Technol. **118**, 251 (2001).
[13] P. A. Cundall and O. D. L. Strack, Géotechnique **29**, 47 (1979).
[14] T. Pöschel and T. Schwager, *Computational Granular Dynamics: Models and Algorithms* (Springer-Verlag, Berlin, 2005).
[15] R. Y. Yang, R. P. Zou, and A. B. Yu, Powder Technol. **130**, 138 (2003).
[16] C. Thornton, S. J. Cummins, and P. W. Cleary, Powder Technol. **210**, 189 (2011).
[17] J. R. Third, D. M. Scott, S. A. Scott, and C. R. Müller, Granular Matter **12**, 587 (2010).
[18] M. Nakagawa, S. A. Altobelli, A. Caprihan, and E. Fukushima, in *Powders and Grains 97*, edited by B. Behringer and J. Jenkins (Balkema, Rotterdam, 1997), pp. 447–450.